Comput. Methods Appl. Mech. Engrg. 266 (2013) 205–218

Contents lists available at SciVerse ScienceDirect

Comput. Methods Appl. Mech. Engrg.

journal homepage: www.elsevier.com/locate/cma

Design of functionally graded piezocomposites using topology optimization and homogenization – Toward effective energy harvesting materials

S.L. Vatanabe [a], G.H. Paulino [b], E.C.N. Silva [a,*]

[a] Department of Mechatronics and Mechanical Systems Engineering, Polytechnic School of University of São Paulo, SP, Brazil
[b] Newmark Laboratory, Department of Civil and Environmental Engineering, University of Illinois at Urbana-Champaign, IL, USA

ARTICLE INFO

Article history:
Received 13 March 2012
Received in revised form 19 June 2013
Accepted 8 July 2013
Available online 18 July 2013

Keywords:
Piezoelectric materials
Topology optimization
Functionally graded materials
Homogenization method
Material design
Polygonal finite elements

ABSTRACT

In the optimization of a piezocomposite, the objective is to obtain an improvement in its performance characteristics, usually by changing the volume fractions of constituent materials, its properties, shape of inclusions, and mechanical properties of the polymer matrix (in the composite unit cell). Thus, this work proposes a methodology, based on topology optimization and homogenization, to design functionally graded piezocomposite materials that considers important aspects in the design process aiming at energy harvesting applications, such as the influence of piezoelectric polarization directions and the influence of material gradation. The influence of the piezoelectric polarization direction is quantitatively verified using the Discrete Material Optimization (DMO) method, which combines gradients with mathematical programming to solve a discrete optimization problem. The homogenization method is implemented using the graded finite element concept, which takes into account the continuous gradation inside the finite elements. One of the main questions answered in this work is, *quantitatively*, how the microscopic stresses can be reduced by combining the functionally graded material (FGM) concept with optimization. In addition, the influence of polygonal elements is investigated, *quantitatively*, when compared to quadrilateral 4-node finite element meshes, which are usually adopted in material design. However, quads exhibit one-node connections and are susceptible to checkerboard patterns in topology optimization applications. To circumvent these problems, Voronoi diagrams are used as an effective means of generating irregular polygonal meshes for piezocomposite design. The present results consist of bi-dimensional unit cells that illustrate the methodology proposed in this work.

1. Introduction

This work proposes a methodology, based on topology optimization and homogenization, to design functionally graded piezocomposite materials that considers important aspects in the material design process aiming at energy harvesting applications, such as the influence of piezoelectric polarization directions and the influence of material gradation between the constituent materials in the unit cell. Usually some gradient is obtained in the manufacturing process of piezocomposites – the proposed methodology can take this feature into account in the design. The homogenization method is implemented using the graded finite element concept, which takes into account the continuous gradation inside the finite elements. Macroscopic and microscopic stress values are compared using the homogenization method when the optimized piezocomposites are subjected to an external load. The variation in polarization direction is implemented by means of a discrete material optimization approach. Quadrilateral 4 node finite element meshes are usually adopted in material design; however, they exhibit one-node connections and are susceptible to checkerboard patterns in topology optimization applications and polygonal elements can be very useful in this aspect. Thus, in this work, Voronoi diagrams are also used as a natural and effective means for generating irregular polygonal meshes. We also compare the influence of quadrilateral and polygonal finite element mesh in the performance of piezocomposites. The results obtained consist of bi-dimensional unit cells that illustrate the methodology proposed in this work.

1.1. Piezoelectric materials

Piezoelectric materials have a crystalline structure that provides them with the ability to transform mechanical strain energy

* Corresponding author.
E-mail address: ecnsilva@usp.br (E.C.N. Silva).

0045-7825/$ - see front matter © 2013 Elsevier B.V. All rights reserved.
http://dx.doi.org/10.1016/j.cma.2013.07.003

into electrical charge and, vice versa, by converting an applied electrical potential into mechanical strain. The term piezocomposite applies to any composite resulting from the combination of any piezoelectric material (polymer or ceramic) with other non-piezoelectric materials, including air-filled voids [1]. Piezocomposite materials provide effective properties (elastic, piezoelectric, and dielectric) leading, in general, to better performance than pure piezoelectric materials. The performance characteristics depend on the volume fractions of constituent materials, its properties, shape of inclusions, and mechanical properties of the polymer matrix in the composite unit cell. In the piezocomposite applications considered in this work, we assume that the excitation wavelengths are so large that the detailed structure of the unit cell is not relevant, and the material may be considered as a new homogeneous medium with "effective" properties. Then, the excitation (vibrational forces, for example) will average out over the fine scale variations of the composite medium, in the same way as averaging occurs in the micron-sized grain structure in a conventional ceramic.

1.2. Energy harvesting

An interesting application of piezoelectric materials is energy harvesting devices. Energy harvesting is a process in which energy, that would otherwise be wasted, is processed and stored for future use by an application. The use of harvested energy could extend the operational life of devices traditionally powered by batteries. *This is particularly advantageous in systems with limited accessibility such as biomedical implants and structures with embedded micro and wireless sensors.* It is feasible that such devices would have the ability to generate their own power from the environment. With advances in design and manufacturing as well as reduced power requirements, the use of energy harvesting methods have become practical and have gained significant popularity [2,3]. The piezoelectric property allows the material to capture mechanical energy from its surroundings, usually ambient vibration, and transform it into electrical energy that can power other devices. The use of piezoelectric materials to capitalize on the surrounding ambient vibrations has seen a dramatic rise due to the direct conversion of energy between mechanical and electrical domains. The interest in piezoelectric energy harvesting is reflected in a number of reviews that have been written in recent years [4,5]. Thus, in this context, designing improved piezocomposites for energy harvesting applications is always a goal to be achieved.

1.3. Functionally graded materials

Functionally Graded Materials (FGM) are composite materials whose properties vary gradually and continuously along a specific direction within the domain of the material. The property variation is generally achieved through continuous change of the material microstructure [6]; in other words, FGMs are characterized by spatially-varying microstructures created by non-uniform distributions of the constituent phases. This variation can be accomplished by using reinforcements with different properties, sizes, and shapes, as well as by interchanging the role of reinforcement and matrix (base) material in a continuous manner. Several authors have highlighted the advantages of the FGM concept applied to piezoelectric structures [7,8], which involve local reduction of thermal and mechanical stress concentration [7,9], improved stress redistribution [7], maximization of output displacement, and increased bonding strength [10]. Among many available techniques, FGMs can be manufactured by using Spark Plasma Sintering (SPS), which has certain features such as high heating efficiency, quick temperature rising, self-cleaning of the surface of the materials and improvement of sintering activation, resulting in fast sintering at a lower temperature [11].

1.4. Homogenization

The homogenization method replaces the piezocomposite by an equivalent homogeneous medium and allows the calculation of its effective properties by considering the topology of the composite microstructure and the properties of its constituents [12]. The homogenization theory for piezoelectricity, considering static case (where the operational wavelength is much larger than the unit cell dimensions), was developed by Telega [13] using the variational method of Γ-convergence. Silva et al. [14–16] presented a method for designing piezoelectric microstructures with high performance characteristics using topology optimization techniques and the homogenization method, including features such as hydrostatic coupling coefficient, figure of merit, and electromechanical coupling factor. Sigmund et al. [17] used topology optimization method to design 1–3 piezocomposites with optimal performance characteristics for hydrophone applications. Buehler et al. [18] applied the homogenization technique to calculate the effective properties of an unit cell incorporating piezoelectric and conventional material. This unit cell was used in a topology optimization problem that maximizes the displacement of an arbitrary point due to an applied electric field, while specifying the structure stiffness. Jayachandran et al. [19–21] used stochastic global optimization combined with homogenization method to obtain the optimal granular configuration of the ferroelectric ceramic microstructure for application in piezoelectric actuators.

In the case of energy harvesting applications, where piezocomposites are used as high quality structural materials that have to satisfy strict engineering requirements, it is necessary to evaluate the stress values in the unit cell when the piezocomposite is subjected to external loads. However, stresses determined by taking the composite as (macro) homogeneous material, denoted by effective stresses, can only reflect the response of the composite to external (macro) environments, ignoring the effects of microheterogeneity. Thus, detailed information of stress distribution is necessary for structural design and optimization. The information is particularly useful in determining material strength and micro cracks/defects in the material. In related work, Guedes and Kikuchi [12] used homogenization to compute stress and strain distributions within composite structures. Ni et al. [22] investigated the microscopic stresses in sphere-reinforced composite and unidirectional fiber-reinforced composites, and calculated the effective stress level determined based on a macro-dimensional scale. They concluded that the effective stresses might be much lower than the actual maximum values occurring in the microstructure. In this method, specific loads are applied to the unit cell and finite element analysis is used to determine the stress distribution and to give the information of stress concentration at interfaces.

1.5. Topology optimization

Topology optimization provides the layout, or topology, of a structure or material such that a prescribed objective is maximized or minimized subjected to design constraints. Topology optimization can be combined with homogenization to design unit cells with complicated shapes. Therefore, a richer class of material properties can be achieved, and new kinds of composite materials can be generated rather than the usual fiber-reinforced or laminate types. Moreover, these new materials may be designed to achieve unusual properties [23–25].

The polarization direction of piezoelectric materials can be defined as design variable in the topology optimization method [26]. In a finite element structure, the direction of local polarization at each element is defined by the angle θ_i on a fixed reference. Thus, the design variables can assume continuous values within a certain pre-defined range. However, a disadvantage of this ap-

proach is that the global solution space becomes non-convex, and hence, the problem of multiple local minima needs to be dealt with [27]. The Discrete Material Optimization (DMO) method combines gradients with mathematical programming to solve a discrete optimization problem. This approach has been introduced by Stegmann and Lund [27], who addressed the orientation problem of orthotropic materials and the material selection problem, as well as problems involving both situations, such as in the case of general composite laminate shell structures. This method can be applied to optimize local polarization directions of piezoelectric materials at each point (an attempt to deal with multiple local minima problems). In this work, the DMO concept is implemented with design variables located at nodes.

1.6. Paper organization

This paper is organized as follows: in Section 2, piezoelectric constitutive equations are presented. In Section 3, the homogenization method applied to piezoelectric materials considering the FGM concept, is described. In Section 4, the topology optimization formulation is presented. In Section 5, the numerical implementation is described, including the implementation of polygonal finite element mesh applied to piezocomposite material design, the DMO concept, and the sensitivity analysis, as well as the discrete problem formulation. In Section 6, numerical examples demonstrating the influence of either quadrilateral or polygonal mesh are shown, as well as the influence of material gradation and piezoelectric polarization direction in the piezocomposite design for high performance. Finally, in Section 7, some conclusions are inferred.

2. Piezoelectric constitutive equations

The stress-charge form of the constitutive relation for piezoelectric media are given by:

$$\begin{aligned}\mathbf{T} &= \mathbf{c}^E\boldsymbol{\varepsilon} - \mathbf{e}\mathbf{E},\\ \mathbf{D} &= \mathbf{e}^t\boldsymbol{\varepsilon} + \boldsymbol{\epsilon}^S\mathbf{E},\end{aligned} \tag{1}$$

where $\mathbf{T}$, $\boldsymbol{\varepsilon}$, $\mathbf{D}$, and $\mathbf{E}$ are respectively the mechanical stress tensor, the mechanical strain tensor, the electric charge vector, and the electric field vector. The term $\mathbf{c}^E$ represents the elastic stiffness tensor, which is evaluated at constant electric field. Terms $\mathbf{e}$ and $\boldsymbol{\epsilon}^S$ are respectively the piezoelectric tensor, and the dielectric tensor evaluated at constant strain.

In this work, a bi-dimensional model is considered. As a convention, the polarization axis of the piezoelectric material is considered in the z (or 3) direction. Besides, a plane-strain assumption is considered for modeling the two-dimensional microstructures. Therefore, assuming the model is in the plane 1–3 (x–z) (y is the normal direction) and that the piezoelectric material employed to build the piezocomposite belongs to the hexagonal 6 mm class, the corresponding plane-strain properties can be obtained by considering $\epsilon_y = 0$ and $E_y = 0$ in Eq. (1), and rewriting them using only the terms ϵ_i, T_i, D_i and E_i for $i = 1$ or 3. A plane-stress model could also be considered; however, it is less realistic than the plane-strain model for representing the composite behavior which is assumed to have an infinite length in the y-direction for the two-dimensional case.

These constitutive equations can also be represented by an alternative form [28]:

$$\begin{aligned}\boldsymbol{\varepsilon} &= \mathbf{s}^E\mathbf{T} - \mathbf{d}\mathbf{E},\\ \mathbf{D} &= \mathbf{d}^t\mathbf{T} + \boldsymbol{\epsilon}^T\mathbf{E},\end{aligned} \tag{2}$$

where $\mathbf{s}^E$ is the compliance tensor under short-circuit conditions, $\boldsymbol{\epsilon}^T$ is the clamped body dielectric tensor, and $\mathbf{d}$ is the piezoelectric stress tensor. The relations among the properties in Eqs. (1) and (2) are [28]:

$$\mathbf{s}^E = \left(\mathbf{c}^E\right)^{-1}, \quad \boldsymbol{\epsilon}^T = \boldsymbol{\epsilon}^S + \mathbf{d}^t\left(\mathbf{s}^E\right)^{-1}\mathbf{d}, \quad \mathbf{d} = \left(\mathbf{s}^E\right)\mathbf{e}. \tag{3}$$

3. Homogenization method applied to FGM piezoelectric materials

In this section, the application of homogenization theory to piezoelectricity, considering FGM concept, is briefly discussed. Considering the standard homogenization procedure, we define the two-dimensional unit cell as $Y = [0, Y_1] \times [0, Y_2]$ and the material functions c^E_{ijkl}, e_{ijk} and ϵ^S_{ij} to be Y-periodic functions:

$$\begin{aligned}&\mathbf{c}^{E\epsilon}(\mathbf{x}) = \mathbf{c}^E(\mathbf{x},\mathbf{y}), \quad \mathbf{e}^{\epsilon}(\mathbf{x}) = \mathbf{e}(\mathbf{x},\mathbf{y}), \quad \boldsymbol{\epsilon}^{S\epsilon}(\mathbf{x}) = \boldsymbol{\epsilon}^S(\mathbf{x},\mathbf{y}),\\ &\mathbf{c}^{E\epsilon}(\mathbf{x},\mathbf{y}) = \mathbf{c}^E(\mathbf{x},\mathbf{y}+Y), \quad \mathbf{e}^{\epsilon}(\mathbf{x},\mathbf{y}) = \mathbf{e}(\mathbf{x},\mathbf{y}+Y),\\ &\boldsymbol{\epsilon}^{S\epsilon}(\mathbf{x},\mathbf{y}) = \boldsymbol{\epsilon}^S(\mathbf{x},\mathbf{y}+Y)\end{aligned} \tag{4}$$

with $\mathbf{y} = \mathbf{x}/\epsilon$ where $\epsilon > 0$ is a parameter with small value that represents the microscale in which the properties are changing (composite microstructure scale), and $\mathbf{x}$ and $\mathbf{y}$ are coordinates associated with macro- and micro-dimensions of the composite material, respectively.

Expanding the piezocomposite displacement $\mathbf{u}$ and electric potential ϕ asymptotically [13], one obtains:

$$\begin{aligned}\mathbf{u}^{\epsilon}(\mathbf{x},\mathbf{y}) &= \mathbf{u}_0(\mathbf{x}) + \epsilon\mathbf{u}_1(\mathbf{x},\mathbf{y}),\\ \phi^{\epsilon}(\mathbf{x},\mathbf{y}) &= \phi_0(\mathbf{x}) + \epsilon\phi_1(\mathbf{x},\mathbf{y}),\end{aligned} \tag{5}$$

where only the first-order variation terms are considered since it is assumed that the operational wavelength is much larger than the unit cell dimensions, and $\mathbf{u}_1$ and ϕ_1 are Y-periodic. The strains and electrical potential gradients are written as:

$$\begin{aligned}\boldsymbol{\varepsilon}^{\epsilon}(\mathbf{x},\mathbf{y}) &= \boldsymbol{\partial}_{\mathbf{x}}\mathbf{u}^{\epsilon}(\mathbf{x},\mathbf{y}) = \boldsymbol{\partial}_{\mathbf{x}}\mathbf{u}_0(\mathbf{x}) + \epsilon\boldsymbol{\partial}_{\mathbf{x}}\mathbf{u}_1(\mathbf{x},\mathbf{y}) + \boldsymbol{\partial}_{\mathbf{y}}\mathbf{u}_1(\mathbf{x},\mathbf{y}),\\ \nabla_{\mathbf{x}}\phi^{\epsilon}(\mathbf{x},\mathbf{y}) &= \mathbf{E}^{\epsilon}(\mathbf{x},\mathbf{y}) = \nabla_{\mathbf{x}}\phi_0(\mathbf{x}) + \epsilon\nabla_{\mathbf{x}}\phi_1(\mathbf{x},\mathbf{y}) + \nabla_{\mathbf{y}}\phi_1(\mathbf{x},\mathbf{y}),\end{aligned} \tag{6}$$

where $\boldsymbol{\varepsilon}^{\epsilon}$ is the mechanical strain and:

$$(\partial_x)_{ij}(\cdot) = \frac{1}{2}\left(\frac{\partial(\cdot)_i}{\partial x_j} + \frac{\partial(\cdot)_j}{\partial x_i}\right), \quad (\partial_y)_{ij}(\cdot) = \frac{1}{2}\left(\frac{\partial(\cdot)_i}{\partial y_j} + \frac{\partial(\cdot)_j}{\partial y_i}\right) \tag{7}$$

After some algebraic manipulations (see [15]), it is possible to get the following equations of the effective (or homogenized) properties:

$$\begin{aligned}\mathbf{c}^E_H(\mathbf{x},\mathbf{y}) = \frac{1}{|Y|}\Bigg\{\int_Y \big[&(\mathbf{I} + \partial_{\mathbf{y}}\boldsymbol{\chi}(\mathbf{x},\mathbf{y})) : \mathbf{c}^E(\mathbf{x},\mathbf{y}) : (\mathbf{I} + \partial_{\mathbf{y}}\boldsymbol{\chi}(\mathbf{x},\mathbf{y}))\\ &+ (\mathbf{I} + \partial_{\mathbf{y}}\boldsymbol{\chi}(\mathbf{x},\mathbf{y})) : \mathbf{e}(\mathbf{x},\mathbf{y})\nabla_{\mathbf{y}}\psi(\mathbf{x},\mathbf{y})\big]dY\Bigg\}\end{aligned} \tag{8}$$

$$\begin{aligned}\mathbf{e}_H(\mathbf{x},\mathbf{y}) = \frac{1}{|Y|}\Bigg\{\int_Y \big[&(\mathbf{I} + \partial_{\mathbf{y}}\boldsymbol{\chi}(\mathbf{x},\mathbf{y})) : \mathbf{e}(\mathbf{x},\mathbf{y})(\mathbf{I} + \nabla_{\mathbf{y}}R(\mathbf{x},\mathbf{y}))\\ &- (\mathbf{I} + \nabla_{\mathbf{y}}R(\mathbf{x},\mathbf{y}))\boldsymbol{\epsilon}^S(\mathbf{x},\mathbf{y})\nabla_{\mathbf{y}}\psi(\mathbf{x},\mathbf{y})\big]dY\Bigg\}\end{aligned} \tag{9}$$

$$\begin{aligned}\boldsymbol{\epsilon}^S_H(\mathbf{x},\mathbf{y}) = \frac{1}{|Y|}\Bigg\{\int_Y \big[&(\mathbf{I} + \nabla_{\mathbf{y}}R(\mathbf{x},\mathbf{y}))\boldsymbol{\epsilon}^S(\mathbf{x},\mathbf{y})(\mathbf{I} + \nabla_{\mathbf{y}}R(\mathbf{x},\mathbf{y}))\\ &- \partial_{\mathbf{y}}\boldsymbol{\Phi}(\mathbf{x},\mathbf{y}) : \mathbf{e}(\mathbf{x},\mathbf{y})(\mathbf{I} + \nabla_{\mathbf{y}}R(\mathbf{x},\mathbf{y}))\big]dY\Bigg\}\end{aligned} \tag{10}$$

where $\boldsymbol{\chi}(\mathbf{x},\mathbf{y})$ is the characteristic displacement of the unit cell, $R(\mathbf{x},\mathbf{y})$ is the characteristic electrical potential of the unit cell, and $\psi(\mathbf{x},\mathbf{y})$ and $\boldsymbol{\Phi}(\mathbf{x},\mathbf{y})$ are the characteristic "coupled" functions of the unit cell. All these functions are Y-periodic. The relationships between $\mathbf{u}_1$ and ϕ_1, and the characteristic functions are given by

$$\begin{aligned}\mathbf{u}_1 &= \boldsymbol{\chi}(\mathbf{x},\mathbf{y})\boldsymbol{\varepsilon}(\mathbf{u}_0(\mathbf{x})) + \boldsymbol{\Phi}(\mathbf{x},\mathbf{y})\nabla_{\mathbf{x}}\phi_0(\mathbf{x}),\\ \phi_1 &= \psi(\mathbf{x},\mathbf{y})\boldsymbol{\varepsilon}(\mathbf{u}_0(\mathbf{x})) + R(\mathbf{x},\mathbf{y})\nabla_{\mathbf{x}}\phi_0(\mathbf{x}),\end{aligned} \tag{11}$$

$$\begin{aligned}\partial_{\mathbf{y}}\mathbf{u}_1(\mathbf{x},\mathbf{y}) &= \partial_{\mathbf{y}}\boldsymbol{\chi}(\mathbf{x},\mathbf{y})\partial_{\mathbf{x}}\mathbf{u}_0(\mathbf{x}) + \partial_{\mathbf{y}}\boldsymbol{\Phi}(\mathbf{x},\mathbf{y})\nabla_{\mathbf{x}}\phi_0(\mathbf{x}),\\ \nabla_{\mathbf{y}}\phi_1(\mathbf{x},\mathbf{y}) &= \nabla_{\mathbf{y}}\psi(\mathbf{x},\mathbf{y})\partial_{\mathbf{x}}\mathbf{u}_0(\mathbf{x}) + \nabla_{\mathbf{y}}R(\mathbf{x},\mathbf{y})\nabla_{\mathbf{x}}\phi_0(\mathbf{x}).\end{aligned} \tag{12}$$

The stress relation of Eq. (1) can be rewritten in terms of the homogenized properties as:

$$\mathbf{T}(\mathbf{x},\mathbf{y}) = \mathbf{c}_H^E(\mathbf{x},\mathbf{y})\mathbf{S} - \mathbf{e}_H(\mathbf{x},\mathbf{y})\mathbf{E}. \tag{13}$$

The strain **S** and the electric field **E** are expanded asymptotically as shown in Eq. (6). From Eq. (8)–(10) it can be noticed that the effective elastic property $\mathbf{c}_H^E$ and the effective piezoelectric property $\mathbf{e}_H$ are defined by homogenizing the microscopic properties $\mathbf{c}^E(\mathbf{x},\mathbf{y})$ and $\mathbf{e}(\mathbf{x},\mathbf{y})$, respectively, in the unit cell Y. Thus, it is possible to evaluate the stress distributed in the unit cell by using Eq. (14) [12,22].

$$\begin{aligned}\boldsymbol{\sigma}(\mathbf{x},\mathbf{y}) = &\left[\mathbf{c}^E(\mathbf{x},\mathbf{y}) : \left(\mathbf{I} + \partial_{\mathbf{y}}\boldsymbol{\chi}(\mathbf{x},\mathbf{y})\right) + \mathbf{e}(\mathbf{x},\mathbf{y})\nabla_{\mathbf{y}}\psi(\mathbf{x},\mathbf{y})\right]\partial_{\mathbf{x}}\mathbf{u}_0(\mathbf{x})\\ &- \left[\mathbf{c}^E(\mathbf{x},\mathbf{y}) : \partial_{\mathbf{y}}\boldsymbol{\Phi}(\mathbf{x},\mathbf{y}) + \mathbf{e}(\mathbf{x},\mathbf{y})\left(\mathbf{I} + \nabla_{\mathbf{y}}R(\mathbf{x},\mathbf{y})\right)\right]\nabla_{\mathbf{x}}\phi_0(\mathbf{x}).\end{aligned} \tag{14}$$

The formulation of the homogenization method is the same for the case with or without material gradation. However, in the FGM case, the properties vary at each position in the unit cell, according to the material gradation (further described in Section 5.3).

4. Topology optimization method

A major concept in topology optimization is the extended design domain, which is a large fixed domain that must contain the whole structure to be determined by the optimization procedure. The objective is to determine the holes and connectivities of the structure by adding and removing material in this domain. Because the extended domain is fixed, the finite element model is not changed during the optimization process, which simplifies the calculation of derivatives of functions defined over the extended domain [29,30]. In the case of material design, the extended design domain is the unit cell domain.

In Fig. 1, the scheme of a topology optimization procedure for piezocomposite material design is presented. Within the initial domain the mesh is generated and the optimization procedure is performed, providing a topology that can be post-processed, verified, and manufactured.

The discrete problem, where the amount of material at each element can assume only values equal to either zero or one (i.e. void or solid material, respectively), is an ill-posed problem. A typical way to seek a solution for topology optimization problems is to relax the problem by allowing the material to assume intermediate property values during the optimization procedure, which can be achieved by defining a special material model [30,31]. Essentially, the material model approximates the material distribution by defining a function of a continuous parameter (design variable) that determines the mixture of basic materials throughout the domain. In this sense, the relaxation yields a continuous material design problem that no longer involves a discernible connectivity. A topology solution can be obtained by applying penalization coefficients to the material model to recover the 0–1 design (and thus, a discernible connectivity), and some gradient control on material distribution, such as a filter or projection [32]. It turns out that this relaxed problem is strongly related to the FGM design problem, which essentially seeks a continuous transition of material properties [33]. Therefore, while the 0–1 design problem (needs complexity control, such as filter) does not admit intermediate values of design variables, the FGM design problem admit solutions with intermediate values of the material field.

Thus, the objective of the present work is to design FGM piezocomposites using the concept of the relaxed problem in continuum topology optimization. The problem consists of maximizing the electromechanical coupling coefficient defined in Section 4.2.

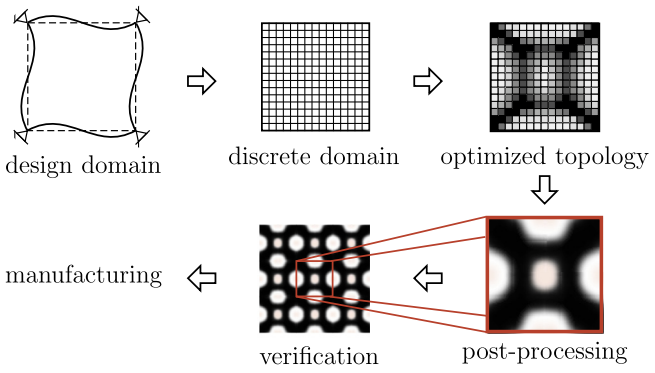

Fig. 1. Steps in the piezocomposite material design using the Topology Optimization Method.

4.1. Material model

In this work, the topology optimization formulation employs a material model based on the SIMP (Solid Isotropic Material with Penalization) model [32], which states that at each point of the domain, the local effective property of the mixture is

$$\begin{aligned}\mathbf{c}^h &= \rho^{p_c}\mathbf{c}_{\mathrm{mat}_1} + (1-\rho^{p_c})\mathbf{c}_{\mathrm{mat}_2},\\ \mathbf{e}^h &= \rho^{p_e}\mathbf{e}_{\mathrm{mat}_1} + (1-\rho^{p_e})\mathbf{e}_{\mathrm{mat}_2},\\ \boldsymbol{\epsilon}^h &= \rho^{p_\epsilon}\boldsymbol{\epsilon}_{\mathrm{mat}_1} + (1-\rho^{p_\epsilon})\boldsymbol{\epsilon}_{\mathrm{mat}_2},\end{aligned} \tag{15}$$

where $\mathbf{c}_{\mathrm{mat}_i}$, $\mathbf{e}_{\mathrm{mat}_i}$ and $\boldsymbol{\epsilon}_{\mathrm{mat}_i}$ correspond to the elastic, piezoelectric, and dielectric tensors of Eq. (1), respectively, for materials 1 and 2. The variable ρ is a pseudo-density describing the amount of material at each point of the domain, which can assume values between 0 and 1. A topology solution can be obtained by applying penalization coefficients p_c, p_e and p_ϵ to the material model to recover the 0–1 design, and some gradient control on material distribution, such as a filter or projection [32]. These penalization coefficients are chosen according to two conditions that the three penalty exponents must satisfy for stable convergence developed by Kim et al. [34]. The first condition is an intrinsic condition ensuring better energy conversion efficiency between mechanical and electric energy for more piezoelectric material usage and the second one is an objective-dependent condition favoring a distinct material distribution over an intermediate material distribution for the same amount of piezoelectric material used.

In order to vary the polarization directions in the unit cell, it is necessary to add more design variables at each point of the design domain, called orientation variable γ_i, which are continuum variables, ranging from 0 to 1, representing each candidate angle of polarization for the piezoelectric material. These variables are further described in Section 5.4.

4.2. Design problem formulation

The optimization problem aiming at energy harvesting applications consists of finding a distribution of material that maximizes the electromechanical coupling coefficient k, which represents the coupling between the directions of stress and electrical fields. It is related to energy in the sense that it is the ratio of the peak energy stored in the "capacitor" of the piezoelectric material to the peak strain energy with electrodes open, and its square is equal to the ratio of the converted electrical energy and the input mechanical energy. Therefore, the electromechanical coupling

coefficient is an important parameter for describing the energy conversion capability of the piezoelectric material, and the optimization problem aiming at energy harvesting applications in quasi-static operation must find the material distribution that maximizes the electromechanical coupling coefficient k, which is given by ([15]):

$$k = \sqrt{\frac{(d_H)^2}{s_H^E \epsilon_{33}^T}}. \tag{16}$$

Thus, the optimization problem can be stated as:

$$\begin{aligned} \underset{\rho(\mathbf{x}),\theta(\mathbf{x})}{\text{Maximize}}: \quad & F(\rho(\mathbf{x}),\theta(\mathbf{x})) = k \\ & 0 \leqslant \rho(\mathbf{x}) \leqslant 1 \\ & -90^\circ \leqslant \theta(\mathbf{x}) \leqslant 90^\circ \\ & \text{symmetry conditions} \\ & \text{gradation control} \end{aligned}$$

where F is the function to be maximized, and $\rho(\mathbf{x})$ and $\theta(\mathbf{x})$ are the design variables at each position $\mathbf{x}$ of the design domain. The values of ρ vary from 0 to 1, representing the presence of material 1 or 2, and the values of θ vary from -90° to 90°, representing the polarization direction of the piezoelectric material at each point.

5. Numerical implementation

A continuum distribution of the design variable inside the finite element domain is considered allowing representation of a continuous material variation during the design process. As the interest here is to obtain solutions with a continuous distribution of material, intermediate materials (no penalization) are allowed. A material model based on the SIMP model together with the DMO concept [27] is applied to verify the influence of the piezoelectric polarization direction in the objective function. A gradient control constraint in the unit cell domain is implemented based on projection techniques [35,36]. This gradient control capability addresses the influence of FGM gradation in the design of graded materials. It also avoids the problem of mesh dependency in the topology optimization implementation [32]. The actual optimization problem is solved by the MMA ("Method of Moving Asymptotes") [37].

In this section, the finite element scheme for convex n-gons outlined in [38] is reviewed and extended to piezoelectric materials. Then, the homogenization method is applied to piezoelectric materials using polygonal elements and material gradation control. After that, the implementation of the DMO concept applied to piezoelectric polarization direction is explained. The sensitivity analysis is presented and, finally, the discrete problem formulation is defined.

5.1. Piezoelectric polygonal element

Most published articles that work with topology optimization method uses the quadrilateral 4 node finite element, also known as Q4. However, the associated meshes exhibit one-node connections and are susceptible to checkerboard patterns in topology optimization applications, which have been the subject of extensive research [39]. Polygonal elements can be very useful in this respect since they can naturally exclude checkerboard layouts [40]. In this work, Voronoi diagrams are used as a natural and effective means for generating irregular polygonal meshes. An attractive feature of the method is that randomness and subsequently higher levels of geometric isotropy are obtained as a byproduct of arbitrary seed placement. Furthermore, the use of Lloyd's algorithm [41] can remove excessive element distortion, and allows construction of meshes that are relatively uniform in size. In this work, the formulation described by Talischi et al. [42–44] is extended to piezoelectric materials. Eqs. (8)–(10) are solved by using the Finite Element Method (FEM). It is assumed that the unit cell is discretized by N finite elements, that is:

$$Y = \bigcup_{n=1}^{N} \Omega^e, \tag{17}$$

where N is the number of finite elements and Ω^e is the domain of each element.

The approach presented by Sukumar and Tabarraei [38] constructs a conforming approximation space on polygonal meshes using natural neighbor bilinear interpolation functions and isoparametric transformations. For $n = 3$ and $n = 4$, the resulting finite element is identical to the constant strain triangle and bilinear quadrilateral, respectively.

Now, consider a set of nodes $\{\mathbf{q}_i\}$ and point $\mathbf{p}$ located where nodal data should be interpolated. Points $\mathbf{p}$ and $\{\mathbf{q}_i\}$ are "natural neighbors" if their Voronoi cells have a common edge [38]. The set of natural neighbors of $\mathbf{p}$ are defined as follows:

$$\mathcal{I}(\mathbf{p}) = \{i | V_i \cap V_p \neq \emptyset\}, \tag{18}$$

where V_i and V_p denote the Voronoi cells of $\mathbf{q}_i$ and $\mathbf{p}$, respectively. The *Laplace interpolant* corresponding to $\mathbf{q}_i$ is given by:

$$N_i(\mathbf{x}) = \frac{w_i(\mathbf{x})}{\sum_{j\in\mathcal{I}} w_j(\mathbf{x})} \quad \text{where } w_i(\mathbf{x}) = \frac{s_i(\mathbf{x})}{h_i(\mathbf{x})}. \tag{19}$$

Here $\mathbf{x}$ is the location of $\mathbf{p}$, s_i is the length of the Voronoi edge common to V_i and V_p, and h_i denotes the distance between $\mathbf{p}$ and $\mathbf{q}_i$, as illustrated in Fig. 2. By construction, the Laplace functions are non-negative, bounded and satisfy partition of unity:

$$0 \leqslant N_i(\mathbf{x}) \leqslant 1, \quad \sum_{i\in\mathcal{I}} N_i(\mathbf{x}) = 1. \tag{20}$$

Furthermore, it can be shown that these functions are linearly precise:

$$\sum_{i\in\mathcal{I}} \mathbf{x}_i N_i(\mathbf{x}) = \mathbf{x}. \tag{21}$$

where $\mathbf{x}_i$ represents the location of node $\mathbf{q}_i$. This property along with constant precision (partition of unity) ensures the convergence of the Galerkin method for second-order partial differential equations. Moreover, Laplace functions are linear on the boundary of the convex hull of $\{\mathbf{q}_i | i \in \mathcal{I}\}$ [45], and satisfy the Kronecker-delta property, meaning that the interpolated value at a node is equal to the nodal value. If the nodes are located at the vertices of a convex polygon, any interior point of this polygon has $\mathbf{q}_i$ as its

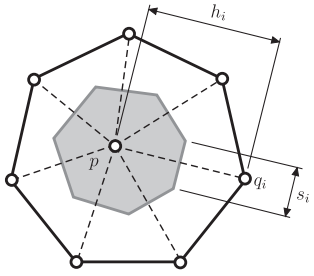

Fig. 2. Schematic drawing showing how to calculate the geometric quantities s_i and h_i used to define the Laplace shape functions.

natural neighbors. Therefore, Laplace shape functions corresponding to $\mathbf{q}_i$ lead to a finite element for that polygon. Furthermore, an isoparametric mapping from regular n-gons to any convex polygon can be constructed using these shape functions. Since the interpolated field varies linearly on the boundary, the resulting approximation is conforming. Following the usual approach in the finite element community, the shape functions are defined on the parent domain, where the weak form integrals are evaluated numerically. The reference n-gon is divided into n triangles (by connecting the centroid to the vertices) and well-known quadrature rules are used on each triangle.

Considering that the topology optimization results in a smoothly graded material, a more natural way of representing the material distribution emerges by considering a continuous representation of material properties [46,47], which is achieved by interpolating the properties inside the finite element using shape functions [35,46,48]. Thus, nodal design variables are defined, rather than the usual element based design variables. Accordingly, the design variable inside each finite element is given by

$$\rho(\mathbf{x}) = \sum_{i=1}^{nn} \rho_i N_i(\mathbf{x}), \tag{22}$$

where ρ_i is the nodal design variable, N_i is the Laplace shape function described above, and nn is the number of nodes at each element. This formulation allows a continuous distribution of material along the design domain instead of the traditional piecewise constant material distribution used by previous formulations of topology optimization [32].

5.2. Homogenization method using polygonal elements applied to piezoelectric materials

Bilinear interpolation functions are considered for displacements and electrical potentials. Therefore, the characteristic functions previously defined are expressed in each element as a function of the shape functions (N_I):

$$\begin{aligned} &\chi_i^{(mn)} \cong N_I \chi_{iI}^{(mn)}, \quad \psi^{(mn)} \cong N_I \psi_I^{(mn)}, \\ &\Phi_i^{(m)} \cong N_I \Phi_{iI}^{(m)}, \quad R^{(m)} \cong N_I R_I^{(m)}, \quad I = 1, NN, \end{aligned} \tag{23}$$

where NN is the number of nodes per finite element (in the case of polygonal elements, it usually varies from 3 to 7). Assembling the individual matrices for each element, we obtain the following global matrix system for each load case mn or m ([15,49,50]):

$$\begin{bmatrix} \mathbf{K_{uu}} & \mathbf{K}_{\mathbf{u}\varphi} \\ \mathbf{K}_{\mathbf{u}\varphi}^t & -\mathbf{K}_{\varphi\varphi} \end{bmatrix} \begin{bmatrix} \boldsymbol{\chi}^{(mn)} & \boldsymbol{\Phi}^{(m)} \\ \boldsymbol{\Psi}^{(mn)} & \mathbf{R}^{(m)} \end{bmatrix} = \begin{bmatrix} \mathbf{F}^{(mn)} & \mathbf{F}^{(m)} \\ \mathbf{Q}^{(mn)} & \mathbf{Q}^{(m)} \end{bmatrix} \Longleftrightarrow \mathbf{KX} = \mathbf{Y}. \tag{24}$$

The stiffness, piezoelectric, and dielectric global matrices ($\mathbf{K_{uu}}$, $\mathbf{K}_{\mathbf{u}\phi}$, and $\mathbf{K}_{\phi\phi}$, respectively) are obtained by assembling each element's individual matrix, and the global force and electrical charge vectors ($\mathbf{F}$ and $\mathbf{Q}$) are the assembly of the element force and electrical charge vectors ($\mathbf{F}^e$ and $\mathbf{Q}^e$, respectively) for all finite elements:

$$\begin{aligned} &\mathbf{K_{uu}} = \sum_{e=1}^{N} \mathbf{K}_{uu}^e, \quad \mathbf{K}_{u\phi} = \sum_{e=1}^{N} \mathbf{K}_{\mathbf{u}\phi}^e, \quad \mathbf{K}_{\phi\phi} = \sum_{e=1}^{N} \mathbf{K}_{\phi\phi}^e, \quad \mathbf{F} = \sum_{e=1}^{N} \mathbf{F}^e, \\ &\mathbf{Q} = \sum_{e=1}^{N} \mathbf{Q}^e. \end{aligned} \tag{25}$$

The element matrices and vectors $\mathbf{K}_{uu}^e, \mathbf{K}_{u\phi}^e, \mathbf{K}_{\phi\phi}^e, \mathbf{F}^e$, and $\mathbf{Q}^e$ are calculated by the following equations [15]:

$$\begin{aligned} &K_{uu(iIjJ)}^e = \int_{\Omega^e} c_{ipjq}^E \frac{\partial N_I}{\partial y_p} \frac{\partial N_J}{\partial y_q} d\Omega^e, \quad K_{u\phi(iIJ)}^e = \int_{\Omega^e} e_{kij} \frac{\partial N_I}{\partial y_j} \frac{\partial N_J}{\partial y_k} d\Omega^e, \\ &K_{\phi\phi(IJ)}^e = \int_{\Omega^e} \epsilon_{ij}^S \frac{\partial N_I}{\partial y_i} \frac{\partial N_J}{\partial y_j} d\Omega^e \\ &F_{iI}^{e(mn)} = -\int_{\Omega^e} c_{ijmn}^E \frac{\partial N_I}{\partial y_j} d\Omega^e, \quad Q_I^{e(mn)} = -\int_{\Omega^e} e_{kmn} \frac{\partial N_I}{\partial y_k} d\Omega^e \\ &F_{iI}^{e(m)} = -\int_{\Omega^e} e_{mij} \frac{\partial N_I}{\partial y_j} d\Omega^e, \quad Q_I^{e(m)} = \int_{\Omega^e} \epsilon_{mj}^S \frac{\partial N_I}{\partial y_j} d\Omega^e. \end{aligned} \tag{26}$$

The displacements and electrical potential at some point of the cell must be prescribed to overcome the non-unique solution of the problem; otherwise the problem will be ill posed. The choice of the point of the prescribed values does not affect the homogenized coefficients because only derivatives of the characteristic functions are used in their computation [15,16].

5.3. Material gradation control

In this work, a gradient control constraint in the unit cell domain is implemented based on the same approach developed by Carbonari et al. [36], which used nodal design variables and projection functions [51]. This gradient control capability addresses the influence of FGM gradation in the design of extreme materials. It also avoids the problem of mesh dependency in the topology optimization implementation when aiming at a discrete solution [32]. This technique adds a new layer of pseudo-nodal material densities (d_n) superimposed on the current layer of nodal design variables (ρ_n). For each design variable ρ_i, a circular area Ω of radius r_{grad} is defined, whose center is located in the same coordinates of the node i, as shown in Fig. 3. The values of ρ_i become a function of the n pseudo-densities values belonging to the circular area Ω, and the distances between each pseudo-density and the center of the area. Thus:

$$\rho_n = f(d_n), \tag{27}$$

where

$$\rho_i = \frac{\sum_{j \in S_i} d_j \alpha(r_{ij})}{\sum_{j \in S_i} \alpha(r_{ij})} \tag{28}$$

in which r_{ij} is the distance between nodes i and j

$$r_{ij} = \|\mathbf{x}_j - \mathbf{x}_i\| \tag{29}$$

and S_i is the subset of the interior nodes in the circular area. The weight factor α is defined by:

$$\alpha(r_{ij}) = \begin{cases} \frac{r_{\text{grad}} - r_{ij}}{r_{\text{grad}}}, & \text{if } \mathbf{x}_j \in S_i, \\ 0, & \text{otherwise.} \end{cases} \tag{30}$$

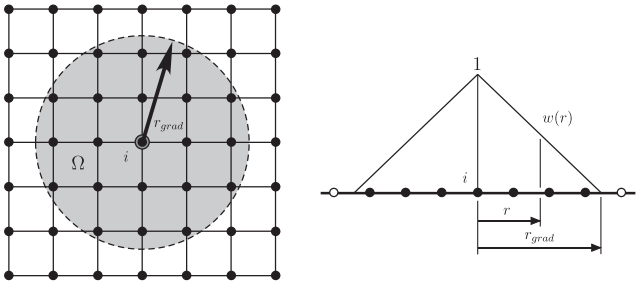

Fig. 3. Projection technique.

5.4. Discrete material optimization (DMO)

The formulation presented by Stegmann and Lund [27], called Discrete Material Optimization (DMO), uses the mixed material strategy suggested by Sigmund et al. [25,52] for multi-phase topology optimization, where the total material stiffness is computed as a weighted sum of candidate materials. In this present work, this method has been applied to optimize polarization direction of piezoelectric materials. For every element in the design domain, this methodology consists of finding a distinct material from a set of candidate materials, such that the objective function is maximized. In the case of polarization direction of piezoelectric materials, each candidate has the piezoelectric properties calculated at a specific polarization angle. Thus, a predetermined number of polarization angles are chosen and the optimization process indicates which one is the best candidate material (see Fig. 4).

The parametrization of the DMO is performed at the finite element level. The piezoelectric tensor of the element, $\mathbf{e}^e$, is expressed as a weighted sum of the piezoelectric tensors of the candidate materials, $\mathbf{e}_i$, as shown in Eq. (31):

$$\mathbf{e}^e_{\mathrm{mat}_j} = \sum_{i=1}^{n^e} w_i \mathbf{e}_i = w_1\mathbf{e}_1 + w_2\mathbf{e}_2 + \cdots + w_{n^e}\mathbf{e}_{n^e}, \quad 0 \leqslant w_i \leqslant 1, \tag{31}$$

where w_i are weighting factors, n^e is the number of finite elements in the design domain, $\mathbf{e}^e_{\mathrm{mat}_j}$ is the resultant piezoelectric tensor of the element e for material j, and $\mathbf{e}_i$ is the piezoelectric tensor of the candidate material i. Each constitutive matrix $\mathbf{e}_i$ can be calculated by the following expression:

$$\mathbf{e}_i = \left(\mathbf{R}_1^{\theta_i}\right)^t \mathbf{e}^0_{\mathrm{mat}_j} \mathbf{R}_2^{\theta_i} \tag{32}$$

and

$$\mathbf{R}_1^{\theta_i} = \begin{bmatrix} c^2 & s^2 & sc \\ s^2 & c^2 & -sc \\ -2sc & 2sc & c^2 - s^2 \end{bmatrix} \quad \text{and} \quad \mathbf{R}_2^{\theta_i} = \begin{bmatrix} c & s \\ -s & c \end{bmatrix}, \tag{33}$$

where $\mathbf{e}^0_{\mathrm{mat}_j}$ is the original piezoelectric matrix of material j without rotation, $s = \sin(\theta_i)$, $c = \cos(\theta_i)$, and θ_i is the discrete angle adopted for each material phase. Index i represents the number of candidate angles and index j represents the number of materials that is distributed in the topology, according to the material model presented in Eq. (15). In the examples adopted in this work, only two types of materials are considered (PZT-5A and epoxy); thus $j = 1, 2$.

The weighting factors w_i in Eq. (31) must have values between 0 and 1 as no piezoelectric tensor can contribute more than the piezoelectric material property, and a negative contribution is physically meaningless. In this way, as in classical topology optimization, the weights on the constitutive matrices become "switches" that turn on and off stiffness contributions such that the objective is minimized and a distinct choice of candidate material is made. At the beginning of the optimization, $\mathbf{e}^e$ consists of contributions from several candidate materials, however, at the end of the design optimization, the parameterization for the weighting functions has to fulfill the demand that one distinct candidate angle is chosen [27]. This underlines the fact that the DMO method relies heavily on the ability of the optimizer to push all weights to the limit values. Any element having intermediate values of the weights must be regarded as undefined because the constitutive properties are non-physical. To achieve this objective, one more design variable need to be adopted, called orientation variable γ_i^e, which is a continuum variable (from 0 to 1) representing each candidate angle. This formulation leads to a high number of variables.

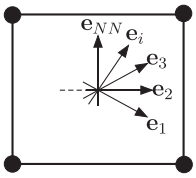

Fig. 4. Example of *NN* candidate materials to be chosen by the optimization process.

With respect to local optimized solutions, Stegmann and Lund [27] investigated this phenomena when the fiber direction in composites are directly handled as design variables. They illustrated this issue by solving a simple problem using a continuous formulation and the method of moving asymptotes (MMA) [37]. The results have shown that the global optimum solution is very dependent on the initial guess. This is not a new realization, of course, and several methods have already been proposed to circumvent the problem of local optimum solutions, such as analytical methods, improved mathematical programming techniques, or parametrization methods. The DMO parametrization is an alternative method that aims to circumvent the local minima problem [27]. Thus, the weighting functions can be calculated by

$$w_i = \frac{\hat{w}_i}{\sum_{k=1}^{n^e} \hat{w}_k}, \quad \text{where } \hat{w}_i = \left(\gamma_i^e\right)^{p_\gamma} \prod_{j=1, j\neq i}^{n^e} \left(1 - \left(\gamma_j^e\right)^{p_\gamma}\right). \tag{34}$$

To push the orientation variables γ_i^e towards 0 or 1, a penalization technique has been adopted by introducing the power, p_γ, to penalize intermediate values of γ_i^e. A low value of p_γ does not guarantee the prevalence of only one polarization direction, what does not make sense from a physical point of view. In addition to that, a high value of p_γ affects the choice of the polarization direction, similarly to what happens in the SIMP model, i.e., the relaxation of the problem is practically removed and the problem may become close to a discrete problem, which is ill-posed. However, there is an heuristic in the choice of this value. In this work, different values of p_γ are previously tested and the best results are obtained for $p_\gamma = 6$. Moreover, the term $\left(1 - \left(\gamma_j^e\right)^{p_\gamma}\right)_{j\neq i}$ is introduced such that an increase in γ_i^e results in a decrease of all other weighting functions. Finally, the weights have been normalized to satisfy the constraint that the sum of the weighting functions is equal to 1. Note that the expression in Eq. (34) means that complicated additional constraints on the design variables γ_i^e are avoided and only simple box constraints have to be dealt with.

5.5. Sensitivity analysis

In this section, the expressions for the sensitivities with respect to the design variables ρ_i (which can be substituted by the design variables d_i) and γ_i^e are presented. The sensitivity analysis provides the gradients of homogenized properties, allowing the optimization solver to set the directions to be taken for each design variable.

The sensitivity with respect to the design variables d_i are obtained using the chain rule:

$$\frac{\partial(\cdot)}{\partial \mathbf{d}_i} = \sum_{j\in\Omega} \frac{\partial(\cdot)}{\partial \rho_j} \frac{\partial \rho_j}{\partial \mathbf{d}_i}, \tag{35}$$

where Ω is the design domain and $\partial\rho_j/\partial d_i$ is not zero only at nodes j belonging to S_i with respect to node i. Furthermore,

$$\frac{\partial \rho_j}{\partial \mathbf{d}_i} = \frac{\alpha(r_{ij})}{\sum_{k\in S_j} \alpha(r_{kj})}, \tag{36}$$

$\partial(\cdot)/\partial\rho_j$ is calculated using traditional methods, such as adjoint method, as described ahead.

The differentiation of the objective function described in Eq. (16) is obtained by using the chain rule. However, the partial derivatives depend on the differentiation of the terms written in Eq. (3), which depend on the differentiation of the homogenized properties of Eqs. (8)–(10). Therefore, the following steps describe how to calculate the sensitivity of the homogenized properties $\mathbf{c}_H^E$, $\mathbf{e}_H$, and $\boldsymbol{\epsilon}_H^S$ as function of the design variables.

By differentiating Eq. (24), one obtains:

$$\frac{\partial \mathbf{K}}{\partial \rho_i}\mathbf{X} + \mathbf{K}\frac{\partial \mathbf{X}}{\partial \rho_i} = \frac{\partial \mathbf{Y}}{\partial \rho_i} \Longleftrightarrow \frac{\partial \mathbf{X}}{\partial \rho_i} = \mathbf{K}^{-1}\mathbf{M}, \quad \text{where}$$
$$\mathbf{M} = \frac{\partial \mathbf{Y}}{\partial \rho_i} - \frac{\partial \mathbf{K}}{\partial \rho_i}\mathbf{X}.$$

For each finite element, we have that:

$$\left\{\frac{\partial \boldsymbol{\chi}^{(mn)}}{\partial \rho_i}\right\}_e = \mathbf{H}_{em}^t \mathbf{K}^{-1}\mathbf{M}^{(mn)} \Rightarrow \left\{\frac{\partial \boldsymbol{\chi}^{(mn)}}{\partial \rho_i}\right\}_e^t = \left(\mathbf{M}^{(mn)}\right)^t \mathbf{K}^{-1}\mathbf{H}_{em}, \tag{38}$$

$$\left\{\frac{\partial \boldsymbol{\psi}^{(mn)}}{\partial \rho_i}\right\}_e = \mathbf{H}_{el}^t \mathbf{K}^{-1}\mathbf{M}^{(mn)} \Rightarrow \left\{\frac{\partial \boldsymbol{\psi}^{(mn)}}{\partial \rho_i}\right\}_e^t = \left(\mathbf{M}^{(mn)}\right)^t \mathbf{K}^{-1}\mathbf{H}_{el}, \tag{39}$$

where $\mathbf{H}_{em}$ is a matrix of $NM \times 5$ filled by 1 at each mechanical degree of freedom and 0 at all others, and $\mathbf{H}_{el}$ is a matrix $NE \times 5$ filled by 1 at each electrical degree of freedom and 0 at all others. Moreover, NM and NE are, respectively, the number of mechanical and electrical degrees of freedom in the entire domain.

By differentiating Eq. (8) with respect to the design variable ρ_i, one obtains [15]:

$$\frac{\partial \mathbf{c}_H}{\partial \rho_i} = \sum_e^N \left\{ (\mathbf{I}+\boldsymbol{\chi})_e^t \left(\frac{\partial \mathbf{K}_{\mathbf{uu}}}{\partial \rho_i}\right)_e (\mathbf{I}+\boldsymbol{\chi})_e + (\mathbf{I}+\boldsymbol{\chi})_e^t \left(\frac{\partial \mathbf{K}_{\mathbf{u}\phi}}{\partial \rho_i}\right)_e \left(\psi^{(mn)}\right)_e \right.$$
$$\left. + \left\{\frac{\partial \boldsymbol{\chi}^{(mn)}}{\partial \rho_i}\right\}_e^t (\mathbf{K}_{\mathbf{uu}})_e (\mathbf{I}+\boldsymbol{\chi})_e + (\mathbf{I}+\boldsymbol{\chi})_e^t (\mathbf{K}_{\mathbf{u}\phi})_e \left(\frac{\partial \psi^{(mn)}}{\partial \rho_i}\right)_e \right\}. \tag{40}$$

The explicit calculation of $\partial \boldsymbol{\chi}^{(mn)}/\partial \rho_i$ and $\partial \psi^{(mn)}/\partial \rho_i$ presents a high computational cost, due to the dependency of all design variables. Thus, the adjoint method is applied to avoid this problem. The third component of Eq. (40) can be rewritten by:

$$\left\{\frac{\partial \boldsymbol{\chi}^{(mn)}}{\partial \rho_i}\right\}_e^t (\mathbf{K}_{\mathbf{uu}})_e (\mathbf{I}+\boldsymbol{\chi})_e = \left(\mathbf{M}^{(mn)}\right)^t \mathbf{K}^{-1}\mathbf{H}_{em}(\mathbf{K}_{\mathbf{uu}})_e (\mathbf{I}+\boldsymbol{\chi})_e$$
$$= \left(\mathbf{M}^{(mn)}\right)^t \mathbf{L}_e \tag{41}$$

and

$$\mathbf{K}\mathbf{L}_e = \mathbf{J}_e, \tag{42}$$

where $\mathbf{J}_e = \mathbf{H}_{em}(\mathbf{K}_{\mathbf{uu}})_e(\mathbf{I}+\boldsymbol{\chi})_e$. By calculating $\mathbf{L}_e$, one can readily compute Eq. (38). Similarly, it is possible to evaluate the fourth component of Eq. (40) by:

$$\left(\mathbf{I}+\boldsymbol{\chi}^{(mn)}\right)_e^t (\mathbf{K}_{\mathbf{u}\varphi})_e \left\{\frac{\partial \boldsymbol{\psi}^{(mn)}}{\partial \mathbf{x}}\right\}_e = (\mathbf{I}+\boldsymbol{\chi})_e^t (\mathbf{K}_{\mathbf{u}\varphi})_e \mathbf{H}_{el}^t \mathbf{K}^{-1}\mathbf{M}^{(mn)} = \mathbf{P}_e^t \mathbf{M}^{(mn)} \tag{43}$$

and

$$\mathbf{K}\mathbf{P}_e = \mathbf{V}_e, \tag{44}$$

where $\mathbf{V}_e = (\mathbf{I}+\boldsymbol{\chi})_e^t (\mathbf{K}_{\mathbf{u}\varphi})_e \mathbf{H}_{el}^t$. Calculating $\mathbf{P}_e$, one promptly computes Eq. (39). In an analogous way, it is possible to calculate the sensitivity of the piezoelectric and dielectric properties by using the adjoint method, reducing the computational cost.

With respect to the DMO formulation, by differentiating Eq. (31), one obtains:

$$\frac{\partial \mathbf{e}_{\mathrm{mat}_j}^e}{\partial \gamma_n^e} = \sum_{i=1}^{n^e} \frac{\partial w_i}{\partial \gamma_n^e}\mathbf{e}_i \quad \text{and} \quad \frac{\partial w_i}{\partial \gamma_n^e} = \frac{\frac{\partial \hat{w}_i}{\partial \gamma_n^e}}{\sum_{k=1}^{n_c} \hat{w}_k}, \tag{45}$$

where

$$\frac{\partial \hat{w}_i}{\partial \gamma_n^e} = \begin{cases} p_\gamma \left(\gamma_n^e\right)^{p_\gamma - 1} \prod_{j=1\, j\neq i}^{n^e} \left(1 - \left(\gamma_j^e\right)^{p_\gamma}\right) & \text{if } n = i, \\ -\left(\gamma_i^e\right)^{p_\gamma} p_\gamma \left(\gamma_n^e\right)^{p_\gamma - 1} \prod_{j=1\, j\neq i, j\neq n}^{n^e} \left(1 - \left(\gamma_j^e\right)^{p_\gamma}\right) & \text{if } n = j. \end{cases} \tag{46}$$

5.6. Discrete problem formulation

The final optimization problem studied can be stated in the discrete form as:

$$\underset{d_i, \gamma_i}{\text{Maximize}}: \quad F(d_i, \gamma_i) = k$$
$$0 \leqslant d_i \leqslant 1, \quad i = 1, \ldots, N$$
$$0 \leqslant \gamma_i \leqslant 1$$
$$\text{symmetry conditions}$$
$$\text{gradation control}$$

where F is the function to be maximized, N is the number of nodes in the design domain, d_i and γ_i are the design variables at each position $\mathbf{x}_i$ of the design domain. The values of d_i vary from 0 to 1, representing the presence of material 1 or 2, and values of γ_i vary from 0 to 1, representing the influence of the polarization direction of the orientation candidate at each node.

A flowchart of the optimization algorithm describing the steps involved is shown in Fig. 5. The method is implemented in MATLAB.

6. Numerical results

In this section, numerical examples of optimized microstructures are provided. First, unit cells are obtained with no material gradation, in order to verify the influence of the finite element mesh and the polarization direction. Later, the same verification is performed again to evaluate the influence of gradation in material design.

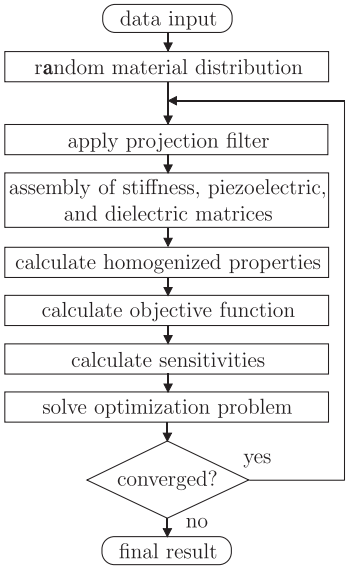

Fig. 5. Flowchart of the optimization procedure.

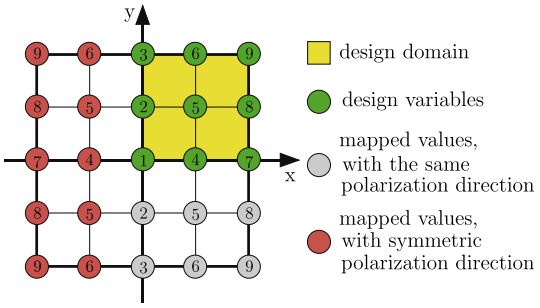

Fig. 6. Illustration of 1/4 unit cell design domain and the mapped nodal values, for a design domain meshed with 2×2 quadrilateral elements.

Table 1
Material properties.

Property	PZT-5A	Epoxy
$c^E_{11}(10^{10}\ \mathrm{N/m^2})$	12.1	0.53
$c^E_{13}(10^{10}\ \mathrm{N/m^2})$	7.52	0.31
$c^E_{33}(10^{10}\ \mathrm{N/m^2})$	11.1	0.53
$c^E_{44}(10^{10}\ \mathrm{N/m^2})$	2.10	0.11
$e_{13}\ (\mathrm{C/m^2})$	−5.4	0
$e_{33}\ (\mathrm{C/m^2})$	15.8	0
$e_{15}\ (\mathrm{C/m^2})$	12.3	0
$\epsilon^S_{11}/\epsilon_0$	1650	4
$\epsilon^S_{33}/\epsilon_0$	1700	4
$\epsilon_0(F/M)$	8.85×10^{12}	

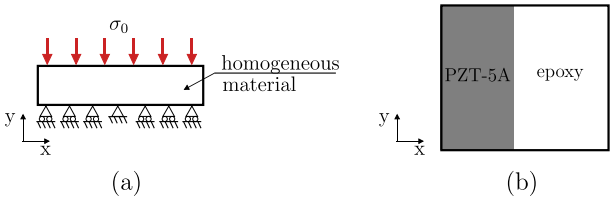

Fig. 7. (a) Macroscopic model adopted to evaluate the stress in the unit cell, and (b) Example of unit cell for the 2–2 piezocomposite.

The adopted design domain is a quarter of a square two-dimensional unit cell, in order to reduce the computational cost. Therefore, before the optimization iterative process starts, it is necessary to perform a mapping scheme of the nodal values along the unit cell, with respect to the design variables in the design domain. For the cases where the polarization direction is fixed in the vertical direction, the material distribution is symmetric with respect to both axes, x and y. For the cases where the polarization direction is included in the optimization, the material distribution is also symmetric in x and y axes; however, the polarization direction is symmetric only with respect to the y-axis. In relation to the x-axis, the polarization direction of the nodal values is identical to the respective design variables. Fig. 6 illustrates this mapping scheme. The simulation is performed taking into account the entire unit cell, applying periodic constraints. The design domain is discretized with 81 elements, so the quadrilateral mesh consists of 9×9 elements and, in the polygonal mesh, the elements are generated according to the corresponding Voronoi diagrams and Lloyd's algorithm (see Section 5.1). The material properties of PZT-5A and epoxy polymer are listed in Table 1. The adopted penalization coefficients of Eq. (15) are $p^c = 2$, $p^e = 2$, and $p^\epsilon = 4$, according to the two conditions that they must satisfy for stable convergence [34].

In this case, the variation of polarization direction of PZT-5A is considered, three different angles are adopted, 0°, 45° and 90°, and therefore, Eq. (31) has three parts, one for each angle. The adopted value for penalization coefficient p of Eq. (34) is equal to 5, to ensure that only one direction is chosen. Approximately 10 full optimization processes are performed for each case, each of them considering a random initial material distribution, in order to alleviate dependency on the initial guess. Then, the best performance obtained for each case is illustrated in this section.

After obtaining the optimized microstructures for each case, homogenized elastic, piezoelectric and dielectric properties are calculated. These homogenized properties are used in a homogeneous macroscopic model to evaluate the macroscopic stress distribution. A uniform pressure σ_0 is applied to the macroscopic model, as shown in Fig. 7a. The adopted two-dimensional macroscopic model consists of a rectangular block of 20×5 mm, made of an homogeneous material, whose properties are the effective properties of each microstructure obtained by the optimization method. This macroscopic model is analyzed by considering plane strain.

From the macroscopic model analysis, the macroscopic strain and the macroscopic electric field are obtained, which are uniform for the entire model. Then, the microscopic stress is calculated for the corresponding unit cell using Eq. (14). The stress distributions inside the optimized unit cells are shown in the following figures.

The electromechanical coupling coefficient of a unit cell made of pure PZT-5A has a value of 0.145. By varying the volume fraction of the 2–2 piezocomposite (see Fig. 7b) with fixed vertical polarization direction, a maximum electromechanical coupling coefficient equal to 0.145 is obtained [15]. The performance of the optimized results presented in Sections 6.1 and 6.2 are compared with the performance of pure PZT-5A and also with the 2–2 piezocomposite. These values are considered as references for the optimized results.

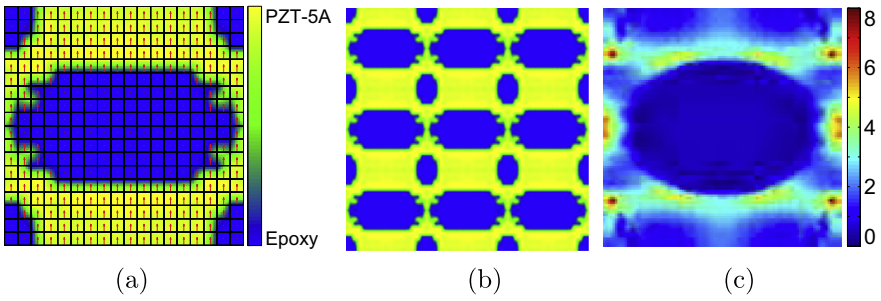

Fig. 8. Optimized microstructure with no material gradation, using quadrilateral mesh and fixed polarization in the vertical direction: (a) material distribution in the unit cell, (b) periodic matrix formed by 3×3 unit cells, and (c) microscopic stress distribution in the unit cell.

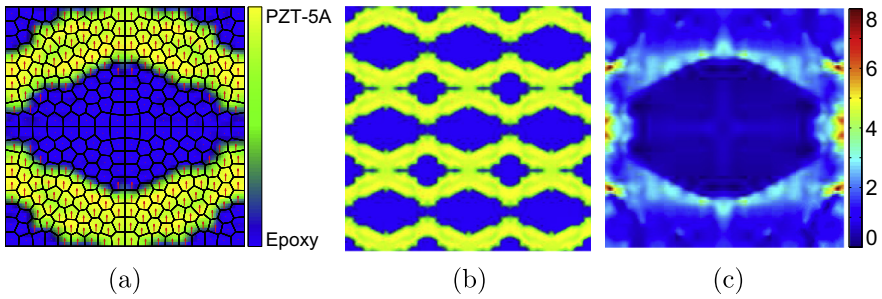

Fig. 9. Optimized microstructure with no material gradation, using polygonal mesh and fixed polarization in the vertical direction: (a) material distribution in the unit cell, (b) periodic matrix formed by 3×3 unit cells, and (c) microscopic stress distribution in the unit cell.

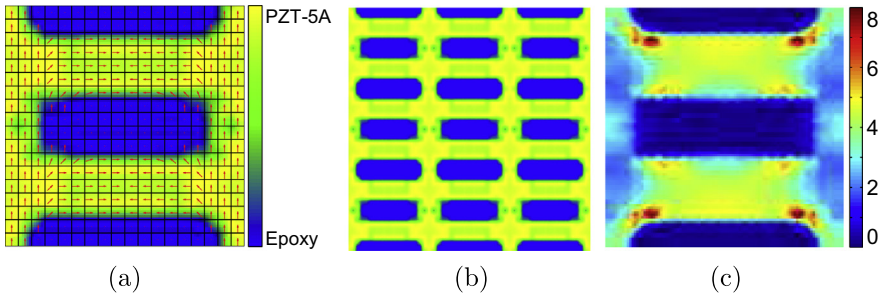

Fig. 10. Optimized microstructure with no material gradation, using quadrilateral mesh and free polarization direction: (a) material distribution in the unit cell, (b) periodic matrix formed by 3×3 unit cells, and (c) microscopic stress distribution in the unit cell.

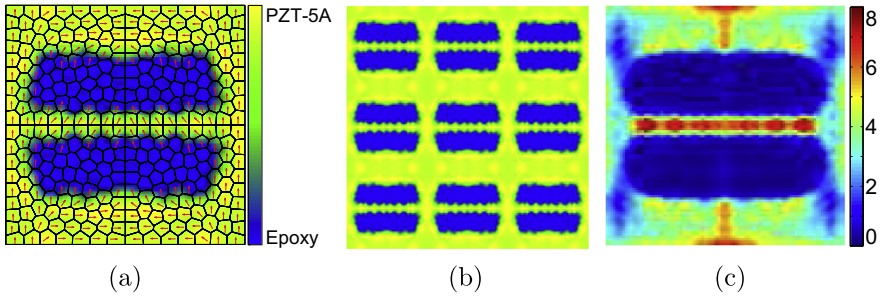

Fig. 11. Optimized microstructure with no material gradation, using polygonal mesh and free polarization direction: (a) material distribution in the unit cell, (b) periodic matrix formed by 3×3 unit cells, and (c) microscopic stress distribution in the unit cell.

Table 2
Homogenized properties of the optimized structures with no material gradation.

Figure	Polarization	Mesh	$\mathbf{c}_H^E$ (MPa)	$\mathbf{e}_H$ (C/m^2)	ϵ_H^E/ϵ_0
8	Fixed	Quad.	$\begin{bmatrix} 38.36 & 16.70 & 0 \\ 16.70 & 27.11 & 0 \\ 0 & 0 & 6.63 \end{bmatrix}$	$\begin{bmatrix} 0 & 0.95 \\ 0 & 4.70 \\ 2.55 & 0 \end{bmatrix}$	$\begin{bmatrix} 906 & 0 \\ 0 & 548 \end{bmatrix}$
9	Fixed	Poly.	$\begin{bmatrix} 31.37 & 15.30 & 0 \\ 15.30 & 22.96 & 0 \\ 0 & 0 & 6.53 \end{bmatrix}$	$\begin{bmatrix} 0 & 1.49 \\ 0 & 3.77 \\ 2.39 & 0 \end{bmatrix}$	$\begin{bmatrix} 764 & 0 \\ 0 & 498 \end{bmatrix}$
10	Free	Quad.	$\begin{bmatrix} 49.55 & 13.05 & 0 \\ 13.05 & 24.37 & 0 \\ 0 & 0 & 4.28 \end{bmatrix}$	$\begin{bmatrix} 0 & -0.05 \\ 0 & 3.96 \\ 0.45 & 0 \end{bmatrix}$	$\begin{bmatrix} 1038 & 0 \\ 0 & 403 \end{bmatrix}$
11	Free	Poly.	$\begin{bmatrix} 59.43 & 17.08 & 0 \\ 17.08 & 29.50 & 0 \\ 0 & 0 & 5.66 \end{bmatrix}$	$\begin{bmatrix} 0 & -0.31 \\ 0 & 4.99 \\ 0.66 & 0 \end{bmatrix}$	$\begin{bmatrix} 1249 & 0 \\ 0 & 508 \end{bmatrix}$

6.1. Optimized non-FGM cell design

Material design examples, using the implemented software, are presented. The first approach is to verify the influence of the type of finite element mesh and the polarization direction in the objective function, considering no gradation in the unit cell. Fig. 8 shows the optimized unit cell for a quadrilateral mesh keeping the polarization in the vertical direction, the periodic matrix formed by 3×3 unit cells, and the microscopic stress distribution in the unit cell. Fig. 9 shows results for a polygonal mesh keeping the polarization in the vertical direction. Figs. 10 and 11 show the optimized results for the quadrilateral and polygonal meshes, respectively,

Table 3
Comparison of optimized non-FGM microstructures.

Figure	Polarization direction	Mesh	k	Gain (%)[a]	σ/σ_0
8	Fixed	Quadrilateral	0.291	100.7	7.8
9	Fixed	Polygonal	0.298	105.5	7.6
10	Free	Quadrilateral	0.309	113.1	7.9
11	Free	Polygonal	0.319	120.0	7.5

[a] With respect to pure PZT-5A ($k = 0.145$).

using the DMO concept, for 0°, 45°, and 90°. The homogenized properties for each case are listed in Table 2.

Table 3 shows the values of k for the four optimized microstructures; their relative gains with respect to the pure PZT-5A or 2–2 piezocomposite, whose values of k are equal to 0.145; and the maximum microscopic relative stress values in the unit cell. The stress distributions presented in these figures are the maximum principal stresses divided by the macroscopic stress value σ_0. Comparing the optimized microstructures with fixed polarization direction, one notices that the polygonal mesh model, with gain of 105.5%, has a better performance than the quadrilateral mesh model, with gain of 100.7%. This effect is repeated for the cases with free polarization direction of Figs. 10 and 11. In this approach, the quadrilateral mesh model has a gain of 113.1%, and the polygonal mesh 120.0%. Moreover, comparing the influence of the polarization direction, it is noted that the performances of the microstructures of Figs. 10 and 11 are better than the performances obtained with fixed polarization direction, presented in Figs. 8 and 9. In the case of Fig. 8, note that the maximum microscopic relative stress values can reach 7.8 times higher than the macroscopic stress σ_0. For the cases of Figs. 9–11, the maximum microscopic stress relative values are 7.6, 7.9, and 7.5 times greater than σ_0, respectively. From these results, one concludes that, by using the same number of finite elements, polygonal meshes guide

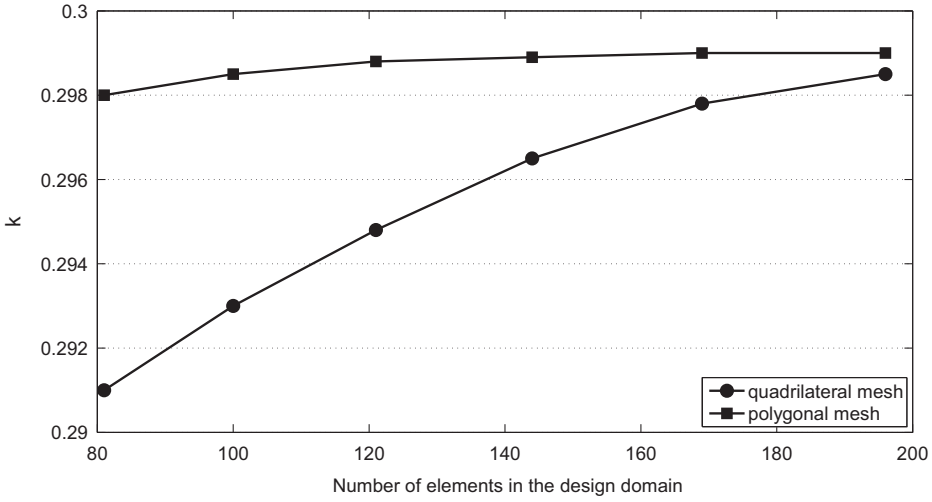

Fig. 12. Mesh convergence analysis.

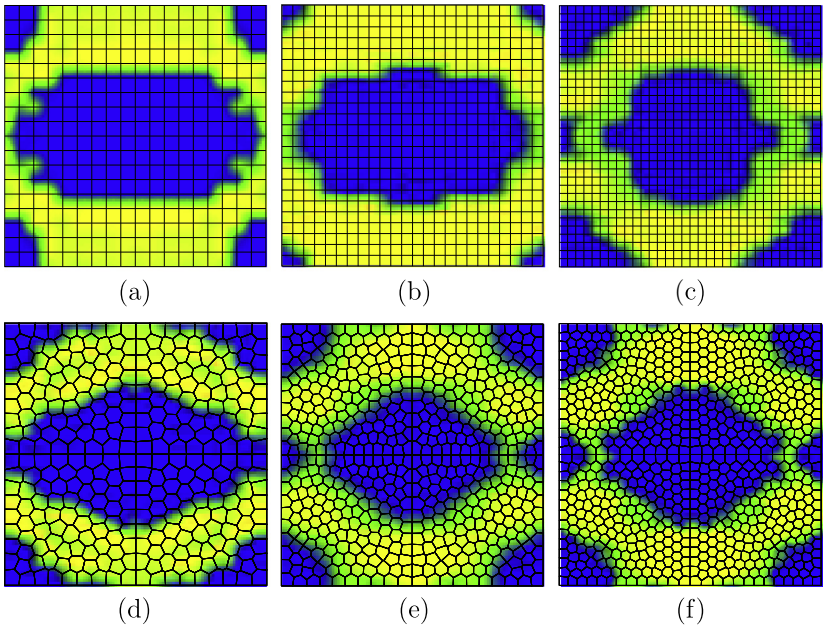

Fig. 13. Mesh convergence analysis. Quadrilateral meshes with (a) 81, (b) 144, and (c) 196 elements. Polygonal meshes with (d) 81, (e) 144, and (f) 196 elements (yellow: PZT-5A; blue: epoxy). (For interpretation of the references to colour in this figure legend, the reader is referred to the web version of this article.)

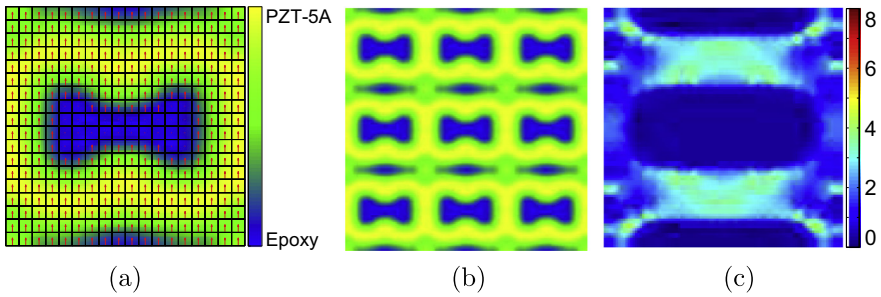

Fig. 14. Optimized microstructure with material gradation, using quadrilateral mesh and fixed polarization direction: (a) material distribution in the unit cell, (b) periodic matrix formed by 3 × 3 unit cells, and (c) microscopic stress distribution in the unit cell.

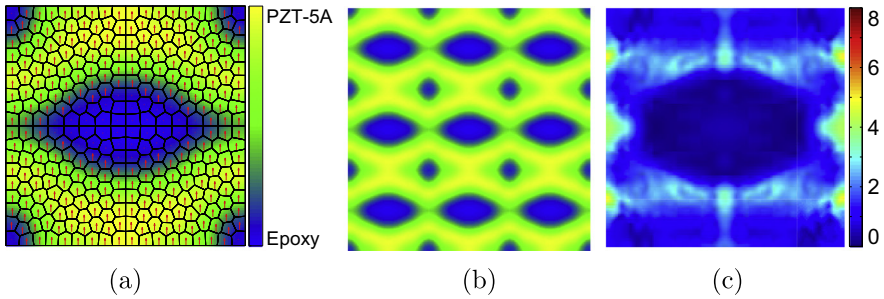

Fig. 15. Optimized microstructure with material gradation, using polygonal mesh and fixed polarization direction: (a) material distribution in the unit cell, (b) periodic matrix formed by 3 × 3 unit cells, and (c) microscopic stress distribution in the unit cell.

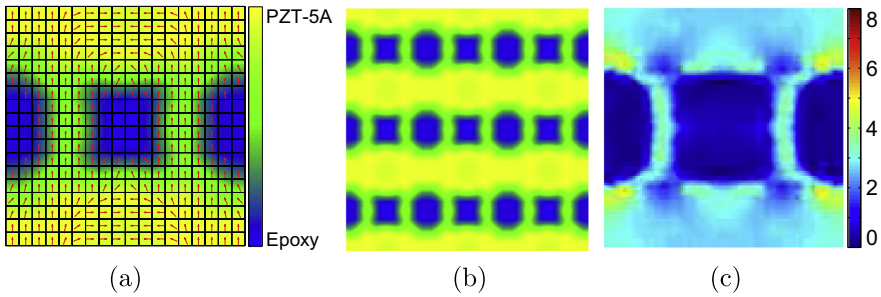

Fig. 16. Optimized microstructure with material gradation, using quadrilateral mesh and free polarization direction: (a) material distribution in the unit cell, (b) periodic matrix formed by 3 × 3 unit cells, and (c) microscopic stress distribution in the unit cell.

the problem toward better local minima. In addition, the variable polarization direction in the unit cell is an important factor and allows microstructure designs with better performance, however with higher stresses.

In order to verify mesh convergence, non-FGM cells are optimized using coarse and refined meshes for both types of elements, quadrilateral and polygonal. The results are shown in Figs. 12 and 13. Fig. 12 presents the convergence of the k value as a function of the number of elements in the unit cell for both cases. For polygonal meshes, the value of k increases slightly with mesh refinement, however, the gain is not significant (less than 0.4%). However, by refining the quadrilateral mesh, a large variation of the k value is verified (approximately 2.7%). Thus, the conclusion obtained from this example is that, by using polygonal meshes, it is possible to satisfy mesh convergence with less elements than quadrilateral meshes. This effect can be seen more clearly in Fig. 13, where three examples for each type of element are shown. By comparing these meshes with the same number of elements, one notices that the quadrilateral meshes have bias in the optimized topology, i.e., the contours of PZT-5A follow the structural meshes, presenting linear boundaries. Rounded contours appear only in more discretized quadrilateral meshes. For polygonal meshes, on the contrary, the contour of PZT-5A is smoothier even with fewer elements.

6.2. Optimized FGM cell design

It is known that materials designed to achieve better performances can only be obtained with solid-void (0–1) designs and steep material variation [53]. However, usually, some gradation is obtained in the manufacturing processes of such materials. Thus, this gradation must be taken into account in the design phase. The same investigation presented previously is performed, considering a gradation radius of 10% of the unit cell length. Figs. 14–17 show the optimized FGM microstructures obtained. The homogenized properties for each case are listed in Table 4.

In Table 5, the values of k for the four optimized microstructures considering material gradations, their relative gains with respect to the pure PZT-5A or 2–2 piezocomposite, and the maximum microscopic stress relative values in the unit cell, are listed. By comparing the optimized microstructures with fixed or variable polarization directions, it is possible to notice that the polygonal mesh models have better performances than the quadrilateral

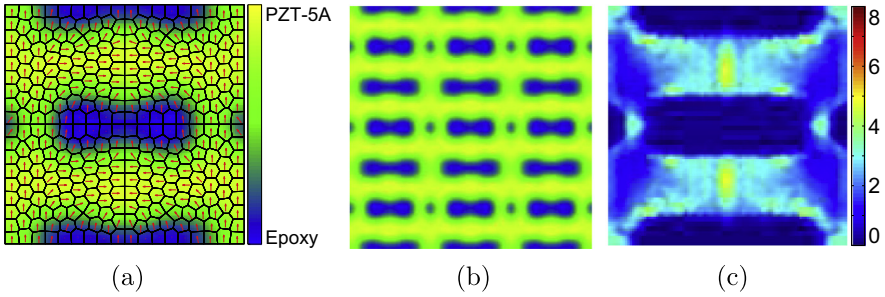

Fig. 17. Optimized microstructure with material gradation, using polygonal mesh and free polarization direction: (a) material distribution in the unit cell, (b) periodic matrix formed by 3 × 3 unit cells, and (c) microscopic stress distribution in the unit cell.

Table 4
Homogenized properties of the optimized structures with material gradation.

Figure	Polarization	Mesh	$\mathbf{c}_H^E$ (MPa)	$\mathbf{e}_H$ (C/m^2)	$\boldsymbol{\epsilon}_H^E/\epsilon_0$
14	Fixed	Quad.	$\begin{bmatrix} 42.68 & 13.32 & 0 \\ 13.32 & 22.92 & 0 \\ 0 & 0 & 4.63 \end{bmatrix}$	$\begin{bmatrix} 0 & 0.04 \\ 0 & 3.60 \\ 1.72 & 0 \end{bmatrix}$	$\begin{bmatrix} 984 & 0 \\ 0 & 402 \end{bmatrix}$
15	Fixed	Poly.	$\begin{bmatrix} 28.25 & 13.48 & 0 \\ 13.48 & 20.93 & 0 \\ 0 & 0 & 5.85 \end{bmatrix}$	$\begin{bmatrix} 0 & 1.24 \\ 0 & 3.05 \\ 2.11 & 0 \end{bmatrix}$	$\begin{bmatrix} 712 & 0 \\ 0 & 378 \end{bmatrix}$
16	Free	Quad.	$\begin{bmatrix} 57.32 & 17.55 & 0 \\ 17.55 & 32.09 & 0 \\ 0 & 0 & 5.36 \end{bmatrix}$	$\begin{bmatrix} 0 & -0.12 \\ 0 & 5.40 \\ 1.32 & 0 \end{bmatrix}$	$\begin{bmatrix} 1209 & 0 \\ 0 & 565 \end{bmatrix}$
17	Free	Poly.	$\begin{bmatrix} 57.66 & 16.52 & 0 \\ 16.52 & 28.76 & 0 \\ 0 & 0 & 5.86 \end{bmatrix}$	$\begin{bmatrix} 0 & -0.28 \\ 0 & 4.63 \\ 0.86 & 0 \end{bmatrix}$	$\begin{bmatrix} 1213 & 0 \\ 0 & 474 \end{bmatrix}$

Table 5
Comparison of optimized FGM microstructures.

Figure	Polarization direction	Mesh	k	Gain (%)[a]	σ/σ_0
14	Fixed	Quadrilateral	0.285	96.6	5.7
15	Fixed	Polygonal	0.294	102.8	5.1
16	Free	Quadrilateral	0.299	106.2	5.9
17	Free	Polygonal	0.305	110.3	6.0

[a] With respect to pure PZT-5A ($k = 0.145$).

mesh models, similarly to the cases with no material gradation presented before. By comparing the maximum relative stress values listed in Table 5, again, polygonal mesh models present smaller values in the microstructure than quadrilateral mesh models. By comparing the influence of material gradation in the maximum relative stress values, one notices that the gain values of k with respect to the pure PZT-5A are smaller than the values obtained with non-FGM microstructures. However, the FGM microstructures, shown in Figs. 14–17, present smaller maximum relative stress values when compared to the non-FGM microstructures shown in Figs. 8–11. Thus, although the objective function values decrease considering material gradation in the unit cell, the maximum microscopic stress values also decrease, which means that the piezocomposite can be subjected to higher loads and thus, a higher amount of energy can be obtained.

7. Conclusions

This work proposes a methodology to design functionally graded piezocomposite materials that considers important aspects in the piezocomposite material design process aiming at energy harvesting applications, such as the influence of piezoelectric polarization directions, the influence of material gradation between the constituent materials in the unit cell, and the influence of either quadrilateral or polygonal finite element mesh in the obtained designs. The variation of the polarization direction is implemented using the DMO concept. From the examples of microstructure designs presented in this work, we conclude that the variable polarization directions in the unit cell are an important factor as it can lead to microstructure designs with better performance. The results presented show that the FGM concept can be applied to design piezocomposite materials with greater performance than pure materials, such as PZT-5A, or 2–2 piezocomposites, for example. As expected, material gradation generates unit cell designs with electromechanical coupling coefficient k values smaller than k values obtained with discrete material distribution. By using the same number of finite elements, polygonal meshes guide the problem toward better local minima than using traditional quadrilateral elements. In addition, by using polygonal meshes, it is possible to satisfy mesh convergence with about 40% less number of elements than quadrilateral meshes. One of the main questions answered in this work is, *quantitatively*, how the microscopic stresses can be reduced by combining the functionally graded material (FGM) concept with optimization (notice that stress concentration is redistributed due to the material gradation in the unit cell). The main conclusion is that although 0–1 structures present higher values of k, they also present higher microscopic stress values; thus sustain lower external loads (to avoid failure) and, consequently, less electrical energy energy can be harvested. On the contrary, although FGM structures present lower values of k, they present lower microscopic stress values; thus sustain higher external loads and, consequently, more electrical energy can be harvested.

Acknowledgments

The first author is thankful for the financial support received from CNPq (National Council for Research and Development, Brazil) and FAPESP (São Paulo State Foundation Research Agency) during his graduate studies through the fellowship No. 2008/57086-6. The second author acknowledges support from the US National Science Foundation under grant number 1321661, and

from the Donald B. and Elizabeth M. Willett endowment at the University of Illinois at Urbana-Champaign (UIUC). The third author is thankful for the financial support received from CNPq, no. 303689/2009-9 and FAPESP research project no. 2011/02387-4. The authors also thank Prof. Svanberg for providing the source code for the Method of Moving Asymptotes (MMA). Any opinion, finding, conclusions or recommendations expressed here are those of the authors and do not necessarily reflect the views of the sponsors.

References

[1] W. Smith, The role of piezocomposites in ultrasonic transducers, Ultrasonics Symposium, 1989 Proceedings, IEEE 2 (1989) 755–766.
[2] S.P. Beeby, M.J. Tudor, N.M. White, Energy harvesting vibration sources for microsystems applications, Measure. Sci. Technol. 17 (2006) R175–R195.
[3] S. Priya, Advances in energy harvesting using low profile piezoelectric transducers, J. Electroceram. 19 (2007) 165–182.
[4] S.R. Anton, H.A. Sodano, A review of power harvesting using piezoelectric materials (2003–2006), Smart Mater. Struct. 16 (2007) R1–R21.
[5] K.A. Cook-Chennault, N. Thambi, A.M. Sastry, Powering MEMS portable devices - A review of non-regenerative and regenerative power supply systems with special emphasis on piezoelectric energy harvesting systems, Smart Materials and Structures 17 (2008) 043001.
[6] Y. Miyamoto, W.A. Kaysser, B.H. Rabin, A. Kawasaki, R.G. Ford, Functionally Graded Materials: Design, Processing and Applications. Kluwer Academic Publishers, Dordrecht, 1999.
[7] A. Almajid, M. Taya, S. Hudnut, Analysis of out-of-plane displacement and stress field in a piezocomposite plate with functionally graded microstructure, Int. J. Solids Struct. 38 (2001) 3377–3391.
[8] G.H. Paulino, E.C.N. Silva, C.H. Le, Optimal design of periodic functionally graded composites with prescribed properties, Struct. Multidiscip. Optim. (2008) 469–489.
[9] B.L. Wang, N. Noda, Design of a smart functionally graded thermopiezoelectric composite structure, Smart Mater. Struct. 10 (2001) 189–193.
[10] J.H. Qiu, K.J. Zhu, H.L. Ji, Fabrication and performance of high temperature style functionally graded piezoelectric bending actuators, Mod. Phys. Lett. B 23 (2009) 433–436.
[11] Z.A. Munir, U. Anselmi-Tamburini, M. Ohyanagi, The effect of electric field and pressure on the synthesis and consolidation of materials: A review of the spark plasma sintering method, J. Mater. Sci. 41 (2006) 763–777.
[12] J.M. Guedes, N. Kikuchi, Preprocessing and postprocessing for materials based on the homogenization method with adaptive finite-element methods, Comput. Methods Appl. Mech. Eng. 83 (1990) 143–198.
[13] J.J. Telega, Piezoelectricity and homogenization: Application to biomechanics, Contin. Models Discr. Syst. 2 (1990) 220–230.
[14] E.C.N. Silva, J.S.O. Fonseca, N. Kikuchi, Optimal design of periodic piezocomposites, Comput. Methods Appl. Mech. Eng. 159 (1998) 49–77.
[15] E.C.N. Silva, J.S.O. Fonseca, F.M. de Espinosa, A.T. Crumm, G.A. Brady, J.W. Halloran, N. Kikuchi, Design of piezocomposite materials and piezoelectric transducers using topology optimization - Part I, Arch. Comput. Methods Eng. 6 (1999) 117–182.
[16] E.C.N. Silva, S. Nishiwaki, N. Kikuchi, Design of piezocomposite materials and piezoelectric transducers using topology optimization - Part II, Arch. Comput. Methods Eng. 6 (1999) 191–222.
[17] O. Sigmund, S. Torquato, I.A. Aksay, On the design of 1–3 piezocomposites using topology optimization, J. Mater. Res. 13 (1998) 1038–1048.
[18] M.J. Buehler, B. Bettig, G.G. Parker, Topology optimization of smart structures using a homogenization approach, J. Intell. Mater. Syst. Struct. 15 (2004) 655–667.
[19] K.P. Jayachandran, J.M. Guedes, H.C. Rodrigues, Piezoelectricity enhancement in ferroelectric ceramics due to orientation, Appl. Phys. Lett. 92 (2008) 232901.
[20] K.P. Jayachandran, J.M. Guedes, H.C. Rodrigues, Homogenization of textured as well as randomly oriented ferroelectric polycrystals, Comput. Mater. Sci. 45 (2009) 816–820.
[21] K.P. Jayachandran, J.M. Guedes, H.C. Rodrigues, Stochastic optimization of ferroelectric ceramics for piezoelectric applications, Struct. Multidiscip. Optim. 44 (2011) 199–212.
[22] A.Q. Ni, Y.W. Zhu, J.H. Wang, Determination of the micro stress field in composite by homogenization method, J. Wuhan Univ. Technol Mater. Sci. Ed. 21 (2006) 114–117.
[23] O. Sigmund, Materials with prescribed constitutive parameters - an inverse homogenization problem, Int. J. Solids Struct. 31 (1994) 2313–2329.
[24] O. Sigmund, Tailoring materials with prescribed elastic properties, Mech. Mater. 20 (1995) 351–368.
[25] O. Sigmund, S. Torquato, Design of materials with extreme thermal expansion using a three-phase topology optimization method, J. Mech. Phys. Solids 45 (1997) 1037–1067.
[26] C.J. Rupp, A. Evgrafov, K. Maute, M.L. Dunn, Design of piezoelectric energy harvesting systems: A topology optimization approach based on multilayer plates and shells, J. Intell. Mater. Syst. Struct. 20 (2009) 1923–1939.
[27] J. Stegmann, E. Lund, Discrete material optimization of general composite shell structures, Int. J. Numer. Methods Eng. 62 (2005) 2009–2027.
[28] ANSI/IEEE, An American national standard – IEEE standard on piezoelectricity, IEEE Trans. Son. Ultrason. 31 (1984) 1–55.
[29] M.P. Bends, N. Kikuchi, Generating optimal topologies in structural design using a homogenization method, Comput. Methods Appl. Mech. Eng. 71 (1988) 197–224.
[30] G. Allaire, Shape optimization by the homogenization method, vol. 146, Applied Mathematical Sciences, New York, 2002.
[31] A. Cherkaev, Variational methods for structural optimization, vol. 140, Springer, New York, 2000.
[32] M.P. Bendsœ, O. Sigmund, Topology Optimization – Theory, Methods and Applications, Springer, New York, USA, 2003.
[33] G.H. Paulino, E.C.N. Silva, Design of functionally graded structures using topology optimization, Functionally Graded Materials VIII 492–493 (2005) 435–440.
[34] J.E. Kim, D.S. Kim, P.S. Ma, Y.Y. Kim, Multi-physics interpolation for the topology optimization of piezoelectric systems, Comput. Methods Appl. Mech. Eng. 199 (2010) 3153–3168.
[35] T.E. Bruns, D.A. Tortorelli, Topology optimization of non-linear elastic structures and compliant mechanisms, Comput. Methods Appl. Mech. Eng. 190 (2001) 3443–3459.
[36] R.C. Carbonari, E.C.N. Silva, G.H. Paulino, Topology optimization design of functionally graded bimorph-type piezoelectric actuators, Smart Mater. Struct. 16 (2007) 2607–2620.
[37] K. Svanberg, The method of moving asymptotes - a new method for structural optimization, Int. J. Numer. Methods Eng. 24 (1987) 359–373.
[38] N. Sukumar, A. Tabarraei, Conforming polygonal finite elements, Int. J. Numer. Methods Eng. 61 (2004) 2045–2066.
[39] O. Sigmund, J. Petersson, Numerical instabilities in topology optimization: A survey on procedures dealing with checkerboards, mesh-dependencies and local minima, Struct. Optim. 16 (1998) 68–75.
[40] C. Talischi, G.H. Paulino, C.H. Le, Honeycomb wachspress finite elements for structural topology optimization, Struct. Multidiscip. Optim. 37 (2009) 569–583.
[41] S.P. Lloyd, Least-squares quantization in PCM, IEEE Trans. Inform. Theory 28 (1982) 129–137.
[42] C. Talischi, G.H. Paulino, A. Pereira, I.F.M. Menezes, Polygonal finite elements for topology optimization: A unifying paradigm, Int. J. Numer. Methods Eng. 82 (2010) 671–698.
[43] C. Talischi, G.H. Paulino, A. Pereira, I.F.M. Menezes, PolyMesher: a general-purpose mesh generator for polygonal elements written in Matlab, Struct. Multidiscip. Optim. 45 (2012) 309–328.
[44] C. Talischi, G.H. Paulino, A. Pereira, I.F.M. Menezes, PolyTop: a Matlab implementation of a general topology optimization framework using unstructured polygonal finite element meshes, Struct. Multidiscip. Optim. 45 (2012) 329–357.
[45] N. Sukumar, B. Moran, A.Y. Semenov, V.V. Belikov, Natural neighbour Galerkin methods, Int. J. Numer. Methods Eng. 50 (2001) 1–27.
[46] K. Matsui, K. Terada, Continuous approximation of material distribution for topology optimization, Int. J. Numer. Methods Eng. 59 (2004) 1925–1944.
[47] S.F. Rahmatalla, C.C. Swan, A Q4/Q4 continuum structural topology optimization implementation, Struct. Multidiscipl. Optim. 27 (2004) 130–135.
[48] S. Rahmatalla, C.C. Swan, Form finding of sparse structures with continuum topology optimization, ASCE J. Struct. Eng. 129 (2003) 1707–1716.
[49] E.C.N. Silva, J.S.O. Fonseca, N. Kikuchi, Optimal design of piezoelectric microstructures, Comput. Mech. 19 (1997) 397–410.
[50] E.C.N. Silva, S. Nishiwaki, J.S.O. Fonseca, N. Kikuchi, Optimization methods applied to material and flextensional actuator design using the homogenization method, Comput. Methods Appl. Mech. Eng. 172 (1999) 241–271.
[51] J.K. Guest, J.H. Prévost, T. Belytschko, Achieving minimum length scale in topology optimization using nodal design variables and projection functions, Int. J. Numer. Methods Eng. 61 (2004) 238–254.
[52] L.V. Gibiansky, O. Sigmund, Multiphase composites with extremal bulk modulus, J. Mech. Phys. Solids 48 (2000) 461–498.
[53] O. Sigmund, A new class of extremal composites, J. Mech. Phys. Solids 48 (2000) 397–428.